Republic of Iraq
Ministry of Higher Education and
Scientific Research
University of Diyala
College of Science
Department of Physics

Synthesis of Zno-Au Nanoparticles by Laser ablation in liquid for Photocatalysis Applications

A thesis
Submitted to the Council of the College of Science, University of Diyala, in partial fulfillment of the requirements for the Master degree in Laser Physics Science

By:

Hanan Khalid Owda

B. Sc. in Physics/ Medical Physics
College of Science/ University of Diyala (2020)

Supervised by:

Prof. Dr. Nadia Mohammed Jassim

2025 AD 1447 AH

ABSTRACT:

In the present work, pulsed laser ablation in liquids (PLAL) of zinc oxide (ZnO), gold (Au) and the ZnO-Au nanoparticles were produced using a 1064 nm Nd:YAG laser. These methods are characterized by their simplicity and the rapid acquisition of nanoparticles with a reduced period of time and cost, while also ensuring high purity and environmentally friendly synthesis conditions.

The structural, morphological, and nonlinear optical characteristics, along with the photocatalytic attributes of the fabricated particles, were investigated employing diverse methods. X-ray diffraction (XRD) findings indicated the crystalline phases of the nanomaterials, with the mean crystallite size measured using the Scherrer equation. Energy-dispersive X-ray spectroscopy (EDX) confirmed the elemental composition of the samples, indicating the presence of only the expected elements and thus verifying the purity of the synthesized nanoparticles, whereas FESEM and TEM images displayed the distinctive shapes of each specimen as spherical gold nanoparticles, hexagonal ZnO nanoparticles, and ZnO-Au nanostructures.

Ultraviolet–visible (UV–Vis) absorption spectra displayed the distinctive surface plasmon resonance of the gold particles and a pronounced absorption edge for the zinc oxide, with notable spectral variations for the ZnO–Au sample attributed to plasmon coupling with the semiconductor. The results of Fourier transform infrared (FTIR) spectroscopy have proved the presence of functional groups and typical bonds in the nanostructures. The nonlinear optical properties of the third-order were studied using a Z-scan technique in closed and open apertures at a 532 nm wavelength. The outcomes demonstrated that the ZnO–Au nanoparticles exhibited greater nonlinear optical susceptibility ($\chi^{(3)}$), nonlinear refractive index (n_2), and nonlinear absorption parameter (β) in comparison to pure ZnO or Au particles. The specimens also exhibited beam self-focusing (positive n_2) and saturated absorption at specific intensities, which were attributed to the LSPR effect of gold and the transmission of charge at the metal-semiconductor interface.

Photocatalytic effectiveness was assessed by examining the breakdown of the methylene blue (MB) stain under sunlight. ZnO-Au nanoparticles demonstrated higher degradation efficiency compared to zinc oxide or pure gold, reaching 91%. This is attributed to the synergistic effect between the enhanced light absorption via the plasmon phenomenon in gold and the photocatalytic activity of zinc oxide. The addition of gold particles also broadened the spectral absorption range and reduced the electron-hole recombination, significantly improving the photocatalytic performance.

In general, this study indicates that PLAL-produced ZnO–Au nanostructures show elevated structural stability, adjustable optical and optical nonlinear characteristics, and excellent photocatalytic effectiveness, rendering them favorable options for utilization in photonic devices, optical power limiters, and environmental pollutant purification. The findings emphasize the potential of green laser-based fabrication techniques for the production of advanced multifunctional nanomaterials.

Chapter One
Introduction and Literature Review

1.1 Introduction

Laser ablation in liquid (LAL) is used to produce nanostructures by ejecting material through laser pulse irradiation onto a solid target, which is placed in liquid. Laser-matter interaction and further ablation highly depend on the pulse energy and its duration, the kind of background liquid, geometry, and morphology of samples, as well as the focusing condition [1]. With this technology, much larger and different materials are minusculely reduced to an atomic size, yielding nanoparticles. Particles in the dimension range of (1 to 100 nanometers) are nanoparticles or NPs. These NPs are really special because of their small size, very high carrier capacity, significant surface area per volume ratio, great reactivity, and easy modification of surface properties[2].

The use of pulsed laser ablation in liquids for nanomaterials fabrication is gradually becoming a chemically very simple and clean technique, presenting the opportunity to have high purity products [3].

Nanoparticles synthesized by laser ablation have been widely used in nonlinear optics, which refers to the intense interaction of light with matter. The optical properties of the sample change nonlinearly, and this effect is called a nonlinear optical effect [4].

The nonlinear optical properties attract researchers and investors to make a plethora of these optical devices, such as lasing, waveguides, all-optical switches, gates, detectors, sensors, spectrometers, microscopes, and storage devices, all because of nonlinear responses and energy gaps [5].

The field of nonlinear optics took off after Franken et al.'s (1961) discovery of the second harmonic generation phenomenon. Monochromatic, directed laser light is used to observe nonlinear optics. The invention of the laser and its beam coherence made it possible to study the behavior of light in optical materials at intensities higher than those of conventional light sources. Therefore, the laser's high intensity enables it to modify the optical properties of materials. Nanomaterials have also received significant attention due to their applications

in various fields such as medicine, the environment, energy, and communications. Thus, the NLO properties of nanomaterial composites have attracted attention due to their applications in optical switching and photovoltaic equipment[6].

The nonlinear optical behavior was evaluated using the Z-scan method [7], as one of the simplest methods. The (1989) invention is used to measure nonlinear absorption coefficient as well as the nonlinear refractive index [4].

The Z-scan method is made up of two techniques, closed-aperture and open-aperture. The Z-scan technique is a closed-aperture technique that relies on measuring the nonlinear refractive index (n_2), including the polarity and magnitude of both the real and imaginary components of the third-order nonlinear optical behavior. In comparison, the open-aperture Z-scan method quantifies the nonlinear absorption coefficient, which encompasses two processes: reverse saturable absorption (RSA) and saturated absorption (SA), depending on such parameters as the pump intensity and the absorption cross-section at the excitation wavelength. The open-aperture Z-scan is specifically useful for assessing the nonlinear absorption coefficient (β). This technique has different types, such as nonlinear media Z-scan, eclipsing Z-scan (EZ-scan), dual-color Z-scan, time-resolved exciting probe Z-scan, and top-hat beam Z-scan[8].

Photocatalyst is a branch of chemistry that uses light and a photocatalyst to stimulate the chemical reactions[9]. Photocatalysis is a Greek-derived term consisting of photo, meaning light, and articulating words into "catalysis", which comes from the verb katergatzai, meaning "to dissolve". It means that a reaction must occur in the presence of a semiconductor illuminated by light[10].

Among all these metal oxides, zinc oxide nanoparticles (ZnO) have received widespread attention due to their catalytic properties, e.g., they possess a significant band gap of 3.37 eV at room temperature, along with a high exciton

binding energy of 60 meV, optical properties, catalytic activity, anti-inflammatory and wound-healing properties, and UV filtering. They have also been used as biosensors for cholesterol, enzyme biochemistry, and biosensing[11].

In addition to the above advantages of zinc oxide catalysts, they are also low cost, photoactive, and widely available. The wide band gap of zinc oxide is a major drawback that makes it less efficient for solar applications, but it is promising for UV detection. However, nanostructures composed of noble metals and zinc oxide can overcome this dilemma. To support visible light detection, metal nanoparticles will absorb visible light and generate localized plasmonic resonances. Therefore, the noble metal gold nanoparticles with a wide band gap semiconductor zinc oxide, are among the most convenient approaches toward enhancing UV-visible photodetection [3].

Gold nanoparticles (Au NPs) are highly regarded for their remarkable capability to strongly absorb electromagnetic waves operating in the visible region through surface plasmon resonance. Together with their ability to remain uniformly distributed in the presence of a matrix, these features have made them a subject of great interest in a variety of fields, such as electronics, sensors, solar cells, medical treatments, drug delivery, and catalysts[12].

1.2 Literature Review

1.2.1 Preparation of Au nanoparticles by the laser ablation method

Year	Investigators	Results
2016	*Guillermo. G, et al*	A pulsed laser was employed to vaporize a gold target submerged in liquid. Spherical gold nanoparticles can be synthesized without the need for any stabilizing ligands, which is one of the major benefits, reducing toxicity, making these nanoparticles appropriate for medical uses[13].
2017	T. Uwada., *et al*	Gold nanoparticles were synthesized in an aqueous solution of HAuCl4, with 1-propanol, using femtosecond (fs) laser-induced cavitation bubbling [14].
2020	M.Nasrollahzadeh., *et al.*	A Q-switched laser was used in water to prepare gold nanoparticles with sizes ranging from 5 to 30 nm. NaBH4 was used as the reducing agent to reduce 4-nitrophenol with 100% efficiency in 20 minutes [15].
2022	M. Ashour., *et al.*	Au NPs were synthesized through laser ablation in pure distilled water, with a nanosecond Nd:YAG laser at a constant 100 mJ energy during 5 or 10 minutes [16].
2023	A. B. Radhi.,*et al.*	The technique of pulsed laser ablation in liquid was used to prepare Au NPs in distilled deionized water. There were two preparation methods: in the first method,

		different specific laser fluxes were used, and the number of pulses was fixed at 300 pulses per flux. In the second method, a different number of laser pulses was used while maintaining a constant laser flux [17].
2025	D. C. Costa, *et al*	Nd:YAG laser, wavelength 1064 nm was used to produce Au NPs by the PLAL method to obtain antibacterial nanoparticles[18].

1.2.2 Preparation of ZnO nanoparticles by the laser ablation method

Year	Investigators	Results
2016	S. V. Farahani,*et al*	Solvents such as methanol and distilled water were used. Analysis revealed a hexagonal crystal structure and varying particle sizes depending on the surrounding environment[19].
2018	G. Al-Dahash,*et al*	A zinc target immersed in sodium hydroxide was used. Scanning electron microscopy (SEM) and ultraviolet-visible (UV-VIS) scanning electron microscopy (SEM) showed a spherical shape, and the peak position moved toward the red region with increasing laser ablation energy [20].
2019	S. I. Al-Nassar,*et al*	The FTIR test showed that the formation of zinc oxide nanoparticles can be indicated by

		absorption values in the range of 435–445 cm^{-1}. The UV-VIS absorption spectra test showed that decreasing the pulse energy reduced the particle size and narrowly distributed them [21].
2019	*W.Zhang, et al.*	ZnO nanoparticles were prepared by focusing laser pulses onto a zinc target immersed in water. The reaction between the zinc plasma and water resulted in the formation of $Zn(OH)_2$, which subsequently decomposed to form the nanoparticles. The effect of laser energy on the particle diameter was also analyzed [22].
2021	*S. S. Khudiar., et al.*	Zinc oxide nanoparticles (ZnO NPs) were prepared using pulsed laser in liquid methanol (PLAL) at different laser energies (400, 600, and 800 mJ). The resulting particles exhibited better electrical conductivity properties compared to silicon and polystyrene crystals.[23].
2024	M. Alwan Kadhum, *et al.*	The method of laser ablation in liquids (PLAL) was used to synthesize zinc oxide nanoparticles (ZnONPs) in distilled water as the medium. The diameters were 35.62 to 80.29 nm on average, and the particles were antibacterial in nature [24].
2025	H. A. Ahmed,.*et al.*	A chemical process is used to create ZnO nanoparticles, which exhibit pertinent anti-

		microbial sensitivity [25].

1.2.3 Preparation of ZnO-Au nanoparticles by the laser ablation method

Year	Investigators	Results
2017	L. D'Urso, *et al.*	Picosecond pulsed laser ablation (ps-PLA) technique was used to prepare ZnO and ZnO/Au nanocolloids [26].
2021	Y. Gündoğdu. *et al.*	High-purity raw materials of zinc oxide (ZnO), gold (Au), and ZnO/Au were subjected to a femtosecond (fs) Ti: Sapphire laser system to form nanoparticles in an ethanolic medium [5].
2021	C. Yao,*et al.*	The liquid-phase pulsed laser ablation technique was used to prepare ZnO-Au nanocomposites by decorating pure zinc oxide with gold nanoparticles [27].

1.2.4 Nonlinear optics of nanoparticles

1.2.4.1 Nonlinear optics of Au (Z- Scan)

Year	Investigators	Results
2022	M. Ashour., *et al.*	It displayed reverse saturable absorption (RSA) characteristics, which increased proportionally with the excitation wavelength and/or incident laser power [16].
2023	B. Azemoodeh Afshar, *et al.*	The Z-scan technique was used, and the data demonstrated that the nonlinear refractive index

		increases with the laser ablation wavelength and strength, while the nonlinear absorption coefficient decreases as the wavelength grows[28].

1.2.4.2 Nonlinear optics of ZnO (Z- Scan)

Year	Investigators	Results
2015	Q. Chang.,*et al.*	ZnO nanoparticles showed a reverse saturable absorption under ns pulses with $n_2=2.14\times10^{-11}$ and 4.79×10^{-13} esu (ns, ps) due to bound electrons [29].
2022	T. Mohamed., *et al.*	The Z-scanning technique was used. The nonlinear absorption coefficient was positive, and the nonlinear refractive index was negative[30].

1.2.4.3 Nonlinear optics of ZnO-Au (Z-Scan) nanoparticles

Year	Investigators	Results
2015	R.Udayabhaskar,*et al.*	By conducting open-aperture Z-scans at 532 nm, it was revealed that the metal nanoparticles modified the optical behavior of the nanocomposites [31].
2016	S. L. Walden, *et al.*	The nonlinear absorption of zinc oxide, zinc oxide-gold hybrids, and zinc oxide-gold mixed colloids were measured by Z-scanning as they

		could potentially be used in optical limiting applications [32].
2020	S. L. Walden., *et al.*	The closed slit using a z-scan was used. The nonlinear refractive index of gold nanoparticles was increased by more than an order of magnitude when they were conjugated with zinc oxide (ZnO) [33].
2021	Y. Gündoğdu.,*et al*	The femtosecond z-scan method was used, and strong nonlinear characteristics were revealed in the near-infrared region [5].

1.2.5 Photo-catalyst ZnO-Au nanoparticles

Year	Investigators	Results
2021	C. Yao.,*et al.*	Zinc oxide-gold nanoparticles exhibit high photocatalytic activity in the ultraviolet and visible regions. Using rhodamine B as a representative organic pollutant, zinc oxide-gold nanocomposites demonstrated excellent photocatalytic performance as visible-light photocatalysts for the degradation of organic pollutants [27].
2022	R. Fiorenza, *et al.*	Good photocatalytic performance of zinc oxide-gold nanostructures has been demonstrated to be efficient in detecting UV and visible light, thus possessing good photocatalytic performance [34].
2023	R. Fiorenza., *et*	The photodegradation efficiency of zinc

	al.	oxide-gold under UV light was about 95% (ZP2) and is used as an antimicrobial [35].

1.3 Aims of the Study

Environmental photocatalysts for wastewater treatment.

Chapter Two
The Theoretical Part

2.1. Introduction

This chapter involves the theoretical part, starting with the solid-state lasers, nonlinear optics, zinc oxide(ZnO), and gold (Au) nanoparticles with their optical properties. Furthermore, the chapter reviews the methods of nanoparticle preparation and photocatalysis activity. Finally, it describes the characterization techniques used for examining the samples.

2.2 Solid State Lasers

Since the Nd:YAG solid-state laser is used for nanoparticle production, only an overview is given:

2.2.1 Nd:YAG Laser

Nd:YAG is defined as a YAG (yttrium aluminum garnet) crystal doped with a small percentage of neodymium, and is one of the most important active media used in solid-state lasers. In this particular lasing medium, the neodymium is a triply ionised dopant that replaces yttrium in the YAG crystal structure[36].

Typically, Nd:YAG lasers emit infrared light with a wavelength of 1064 nm. Nevertheless, transitions can also be seen close to 940, 1120, 1320, and 1440 nm. Nd:YAG lasers have two modes of operation: pulsed and continuous[37].

The 1064 nm Nd:YAG laser is one of the most common types of lasers and is used in a variety of applications. The wavelength of the light that the laser emits is 1064 nm, but it can be tripled (400 nm, blue) or doubled (532 nm, green). Nd:YAG lasers can function in either continuous wave (CW) or pulsed modes. The creation of optical pulses with exceptionally high peak energy is possible using pulsed Nd:YAG lasers, which normally operate in Q-switched mode with pulse widths in the range of nanoseconds (ns)[38].

The Nd:YAG laser consists of a four-level laser system with two pumping bands. The upper band has broad absorption and allows the lamp to be pumped across a wide range of wavelengths in the visible spectrum, while the narrow

absorption band at 808 nm is used for diode pumping using aluminum gallium arsenide semiconductor lasers. The neodymium atoms in both pumping bands rapidly descend to the metastable upper laser level, then emit radiation at 1064 nm when they move to the lower laser level, which is rapidly discharged [39], as shown in **Fig.2.1**.

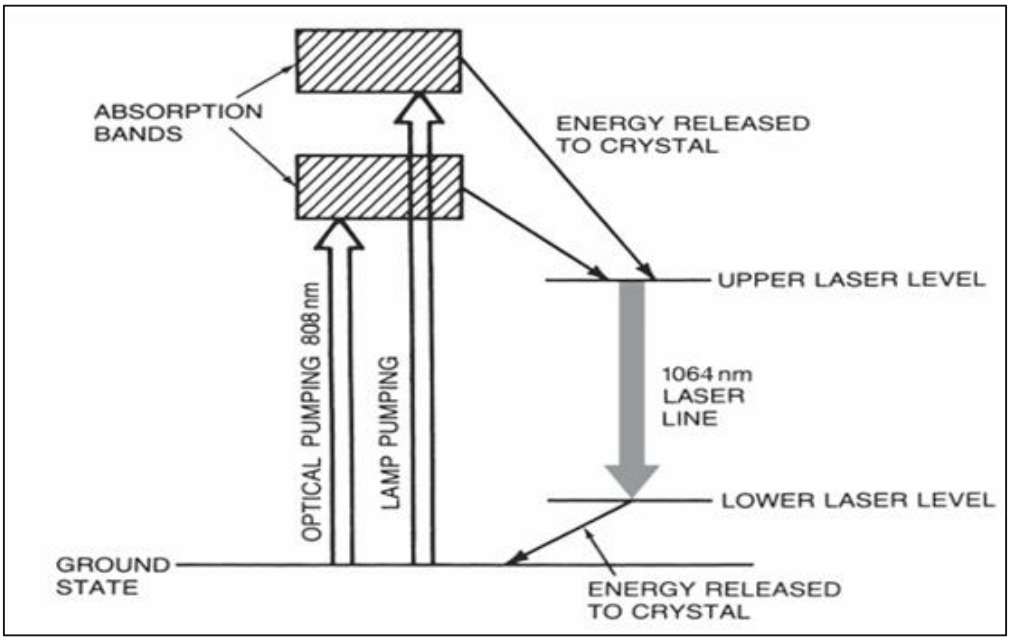

Fig.2.1: Laser energy levels in neodymium, showing pumping both with lamps and with 808 nm diode laser[56]

2.3 The operation mode status of the laser

1-Continuous Operation (CW Mode)

In this setup, the laser produces a continuous, time-steady light beam, with excitation occurring continuously to keep the population inversion condition. This mode has stable output and is suited for uses requiring a constant beam, although the instantaneous power is somewhat low compared to pulsed arrangements[40].

2-Pulsed mode

Within this configuration, sporadic light flashes are produced by the laser, where the energy resides within the active substance and is discharged in brief

spurts. This approach is often employed in tasks needing greater immediate power compared to uninterrupted operation, like precise boring or the investigation of swift occurrences[40].

3- Q-switching mode

This method relies on controlling the optical cavity quality using elements like Pockels cells or acousto-optic modulators. The laser generation is temporarily blocked while the population inversion accumulates, then production is suddenly permitted, leading to the emission of very short pulses (in the nanosecond range) with very high peak power. This style is among the most common ways to obtain high-energy pulses[40].

2.4 Nonlinear optics

In modern optics, nonlinear optics at the nanoscale is one of the most pivotal advances. Its beginnings date back to the advent of the laser, which paved the way for the first practical application of nonlinear optical phenomena: second harmonic generation (SHG)[41].

It is considered an important branch of optics, where amazing phenomena and applications are observed as a result of the effect of the strong electric fields on matter. Induced polarization is not proportional to the applied electric field when a strong electric field is applied to a material because the movement of the electrons relative to their equilibrium positions is very large [42].

Understanding how the polarization (t) of the material changes with the applied electric field intensity (E(t)) related to the electromagnetic field, helps one to comprehend optical nonlinearity. The material becomes non-zero polarized as a result of the atoms or molecules being excited by the external electric field. The induced electric polarization is proportional to the strength of the applied electric field when it is low [6].

$$\mathbf{P}(t) = \chi^{(1)}\mathbf{E}(t) \qquad (2.1)$$

Where: $\chi^{(1)}$ is the linear optical susceptibility.

Nonlinear interaction happens when the electric field is very strong.

The following is a description of the nonlinear optical effects as induced polarization (t) as a power series in the field strength (t):

$$p(t) = \chi^{(1)}E(t) + \chi^{(2)}E_2(t) + \chi^{(3)}E_3(t) + \cdots \qquad (2.2)$$

Where $\chi^{(2)}$ and $\chi^{(3)}$ are referred to as second and third order nonlinear optical susceptibilities, respectively.

Field-dependent changes in optical constants, such as absorption and refractive index, are evidence of optical nonlinearity in optical media, a phenomenon typically associated with the emergence of new optical frequencies. In this regard, the mechanism responsible for the change in optical constants is a method of classifying the nonlinear optical response to materials. Electron-induced optical nonlinearity, thermally induced optical nonlinearity, and external field-induced optical nonlinearity are among the most well-known types of optical nonlinearity[43]. Nonlinear optical procedures are classified into two principal groupings: nonlinear absorption and nonlinear refraction. In nonlinear absorption methods, absorption rises or falls with varying intensity. A specific use of nonlinear absorption, where absorption grows with increasing intensity, is the application of nanoscale optical modulators. These materials permit low-intensity light to go through yet obstruct high-intensity light via nonlinear absorption. Efficient optical modulators are of specific importance for delicate optical instruments and biological uses, where harm may arise at high intensities. Previously, semiconductors have been investigated for their uses at the optical boundary. Owing to their specific and adjustable bandgap, semiconductor nanoparticles can retain high transmittance at low concentrations and, as these densities rise, permit nonlinear absorption throughout the semiconductor bandgap. Prior studies have recognized the potential to improve the optical characteristics of semiconductors by combining them with metal

nanoparticles. This improvement has also been utilized to amplify nonlinear optical effects, like second harmonic generation and nonlinear absorption. Zinc oxide (ZnO) is employed because of its broad band gap of 3.4 eV, which relates to its emission at a wavelength of 370 nm, its elevated transmittance to visible light, and its considerable nonlinear sensitivity. It is likewise a biocompatible substance, rendering it appealing for medical and healthcare uses. This blend of characteristics has prompted substantial interest, as prior research examining the coupling of ZnO to metals has demonstrated the potential to attain notable enhancements in nonlinear refraction and absorption readings[32].

2.4.1 Second-Harmonic Generation (SHG)

SHG is a nonlinear optical phenomenon, where two photons with the same frequency combine to produce a new photon with twice the frequency. This phenomenon is vital in numerous optical technologies, both for commercial and research purposes [44]. SHG is typically observed in materials that lack inversion symmetry, such as non-centrosymmetric crystals, and is used in imaging techniques to produce high-resolution images of materials like 2D semiconductors, transition-metal dichalcogenides, and biological tissues [45]. Additionally, SHG plays an important role in the development of nanodevices for light control and generation at the nanoscale, as it facilitates the coherent combination of different light harmonics[44]. In the case of silicon photonics, SHG is difficult to achieve due to the centrosymmetric structure of group-IV semiconductors like silicon and germanium. Nonetheless, strong SHG has been demonstrated in Ge-rich quantum wells on silicon wafers by breaking symmetry through asymmetric coupled quantum wells, which results in significant nonlinear susceptibility[46].

Besides, the second-harmonic generation (SHG) yields can be amplified many times in ultrathin dielectric nanolaminates, an effect that can be produced by the

collective action of several surfaces. The theoretical works [47] that have used the transfer matrix have predicted that this has increased. Moreover, in monolayer heterocrystals such as MoS_2 and WS2, SHG can be dramatically affected by optical interference between the coherent SH fields, suggesting the possibility to tailor-design parametric generation in such materials[48]. Overall, SHG is a very broad and extremely sensitive tool in the optics field today, and there are near-endless applications of it not only in imaging and material or structure characterization, but also in the development of new photonic technologies.

2.4.2 Sum and Difference Frequency Generation

Sum and difference frequency generation (SFG and DFG) are two phenomena of nonlinear optics that involve the production of new frequencies of light by adding or subtracting the frequency of two incident beams of light. These processes are important in numerous subjects, including the development of new light sources and the exploration of molecular structures. In hole-valley-photonic-crystal-like topological system, the SFG and the DFG can be implemented based on the nonlinear coupling between high-Q corner modes in dual topological band gaps, and their combination offers protection against fabrication defects and high conversion efficiency. The topology enhances flexibility in manipulating the corner modes, and this can be important in meeting exact matching frequencies[49][50].

In contrast, the nonlinearity of the motion equations and a boundary mechanism due to such phenomena as CH displacement are used in conventional methods, including the case of coaxial loudspeakers, to produce sum and difference frequencies, the latter type being far more dominant[51]. Also, SFG and DFG are treated similarly in the classical theory of cylindrical nonlinear optics, which uses exact solutions of the Maxwell equations, and are

therefore analogous to classical coupled-wave equations. SFG and DFG have been further generalized to probe chirality in molecular X-ray spectroscopy, a valuable tool to directly extract local structural asymmetries and develop two-dimensional chirality-sensitive spectroscopy [52][53]. Such developments illustrate the power and capability of both SFG and DFG, capabilities which span the applications spectrum; robust on-chip applications to detailed molecular studies.

2.4.3 Sum-Frequency Generation (SFG)

Sum-Frequency Generation (SFG) is also a nonlinear process in optics, but is considered very surface/interface specific as it crucially involves broken centrosymmetry, typically only available at surfaces.

In SFG, two incident light photons are used to create one outgoing light photon having a frequency equal to the sum of the frequencies of the incident two photons, and thus it is a valuable tool in the study of structures of molecules at interfaces. In the context of surface science, the technique can be especially useful because it can provide interface-selective information (not possible in bulk due to its inversion symmetry, which prohibits SFG under the guidelines of the dipole approximation)[54].

SFG has the problem of poor signal detection, and stronger signals can be achieved with structure-sensitive techniques (like postsample amplification with a picosecond noncollinear optical parametric amplifier (NOPA), which can amplify the SFG signal by several orders of magnitude)[55]. The application of FG to a wide range of materials is enabling a molecular level insight into complex interfacial phenomena that is both nondestructive and in situ[56].

Further developments to SFG have been made, like the use of tunable picosecond IR pulses to gain better spectral resolution in order to explore the phonon modes and other vibrational properties of non-centrosymmetric

media[57]. SFG vibrational spectroscopy is a vital tool in probing the chemistry and physics of surfaces and interfaces of a wide variety of materials.

2.4.4 Optical Parametric Oscillation (OPO)

Optical Parametric Oscillators (OPOs) are adaptable systems that transform laser light to various wavelengths via nonlinear optical methods and present substantial benefit in numerous conventional tasks, e.g., spectroscopy, quantum optics, and imaging. The embedding of OPOs within silicon nitride waveguides has demonstrated greater nonlinearity, pump energy conservation, and compact stable on-chip implementation, which are key features in the development of integrated photonic subsystems[58].

In the application to spectroscopy, singly resonant continuous-wave OPOs are becoming invaluable as a source of tunable, narrow-linewidth idler pulses in the mid infrared region, needed to probe and control molecular vibrations[59]. Also, the ability to use dynamically tuned arrays of polariton parametric oscillators, using surface acoustic waves, has shown the potential in a highly scalable on-chip nonlinear system that benefits from enhanced nonlinearities and dynamic tuning abilities[60]. Quantum optics makes use of OPOs to create entangled photons and squeezed states, which are essential to quantum communication and precision sensing applications[61].

Also, strides made in fiber-based OPOs, especially with the use of photonic crystal fibers, have resulted in devices more useful in the clinical setting, such as coherent Raman imaging by enabling simultaneous pulse trains, high power, and small line widths [62]. These advances speak to the variation and continued advances of the technology of OPOs, and their significance in a variety of fields of science and technology.

2.4.5 Third-Harmonic Generation (THG)

THG is a nonlinear optical process that is critical to many areas, including wavelength conversion, ultra-accurate material characterization, and biological imaging. Recently, the research has focused on making THG more efficient, and more materials and methods have been explored. In another example, an even more dramatic frequency conversion efficiency (320-fold) improvement was demonstrated in a study on a perovskite metasurface relying on the concept of bound states in the continuum (BIC)[63].

Furthermore, sapphire, an extremely transparent material because of its great optical transmission and stability, has been explored on its THG potentialities with the possibility of use being felt on the surface quality inspection of surface materials and real-time inspections on material integrity[64]. The field of biological imaging has more recently led to advances in THG microscopy with the use of synthetic aperture holographic methods. These techniques enable the reconstruction of complex THG signal fields and correct the optical aberrations, resulting in a higher accuracy and better resolution in imaging[82,83].

Furthermore, THG is used to study dielectric materials at or above their laser-induced damage threshold, providing considerable information about their nonlinear optical characteristics and the processes that damage the material[66]. Collectively, these findings reflect the recent flexibility and broadening uses of THG, enabled by materials science and imaging developments.

2.5 Z-Scan technique

Z-scanning is the method in which just one, highly focused laser beam is used as the probe as well as the pump beam. The sample that will be analyzed is transported in the direction of propagation of the laser and across the focus. The closer the sample is to the focus, the smaller the beam size and, therefore, its intensity gets in the sample. This leads to the occurrence of NL optical

phenomena, including self-lensing, saturation of absorption, and MPA. The NL optical properties of many materials, such as crystals, semiconductors, organic dyes, and solutions, have been characterized using Z-scanning[67]. The Z-scan experimental equipment comes in two different variants. The first is the closed aperture technique, which uses an aperture to keep some of the light that the sample transmits from getting to the detector. The second method is the open aperture technique, which involves removing the aperture to gather all of the light [6]. **Fig. 2.2** illustrates the Z-scan experiment setup.

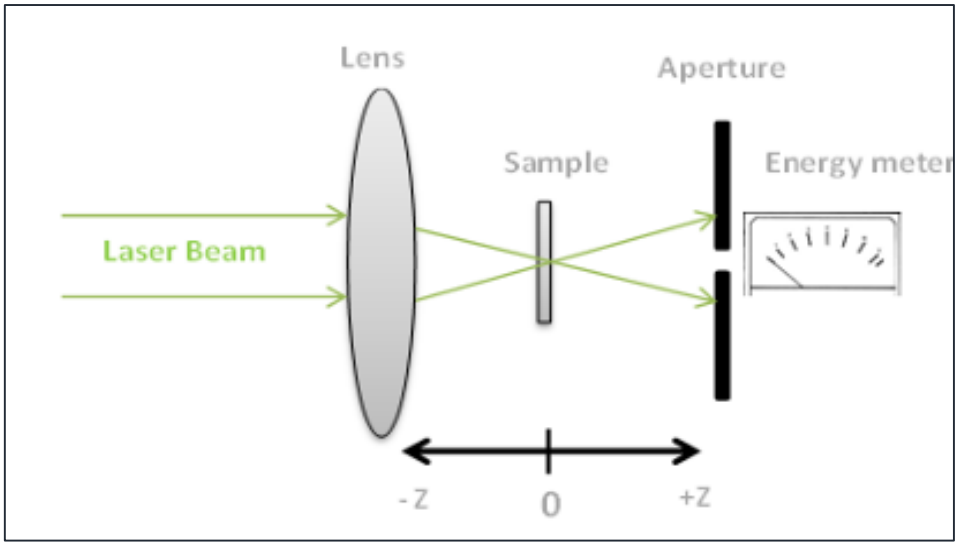

Fig. 2.2:Z-scan experiment setup[68].

2.5.1 Closed aperture Z-scan

In **Fig.2.3**, the amount of a beam focused by lens L is determined using a closed aperture Z-scan. As the sample passes across the focal plane, the intensity varies. The photo detector PD gathers light in the far field that passes through an axially centered aperture A[69].

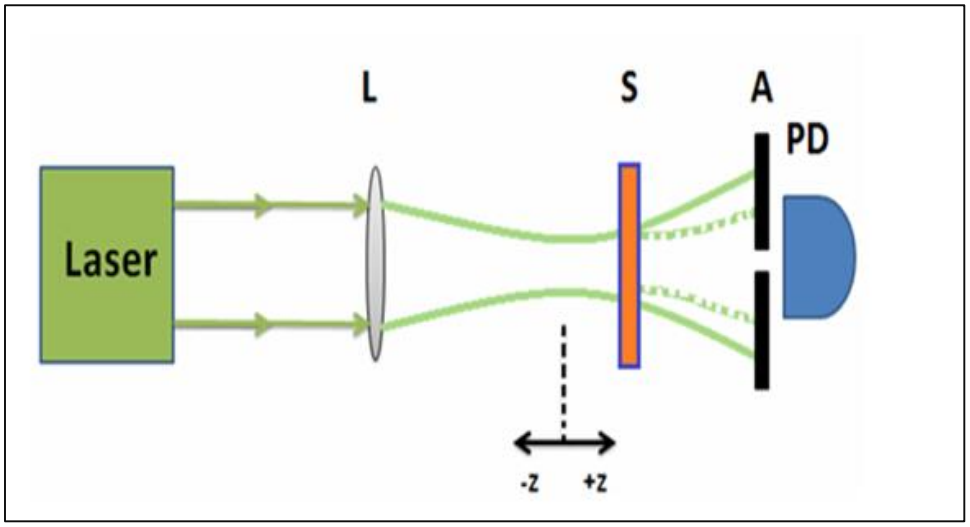

Fig.2.3: Closed aperture Z-scan[69].

To illustrate the connection between the sample's nonlinear refraction and the Z-scan transmittance as a function of Z, when the nonlinear refractive index of the medium is negative and the medium's thickness is smaller than the diffraction length of the focused beam. This could be considered to be a miniature lens with a variable focus length. The initial position (Z_0) far away will lead to minimal beam irradiance and minimal nonlinear refraction. The measured transmittance remains constant since it is z-independent. The sample self-lenses as it approaches the beam focus because of an increase in irradiance. Transmittance measured at the ray position will increase if there is a negative self-lens before the focal plane, which tends to collimate the beam on the aperture in the far field. By increasing the beam divergence after the focal plane, the same self-defocusing causes the beam to broaden at the aperture, which lowers the measured transmittance. The transmittance is z-independent when the nonlinear refraction is low, which is far from focus (z >0). The presence of a transmittance maximum (peak) and transmittance minimum (valley) in the z-scan signature means that the nonlinearity is negative. A positive nonlinearity is found when an inverse scan of the z-curve switches between a peak and a valley[70], as illustrated in **Fig.2.4**.

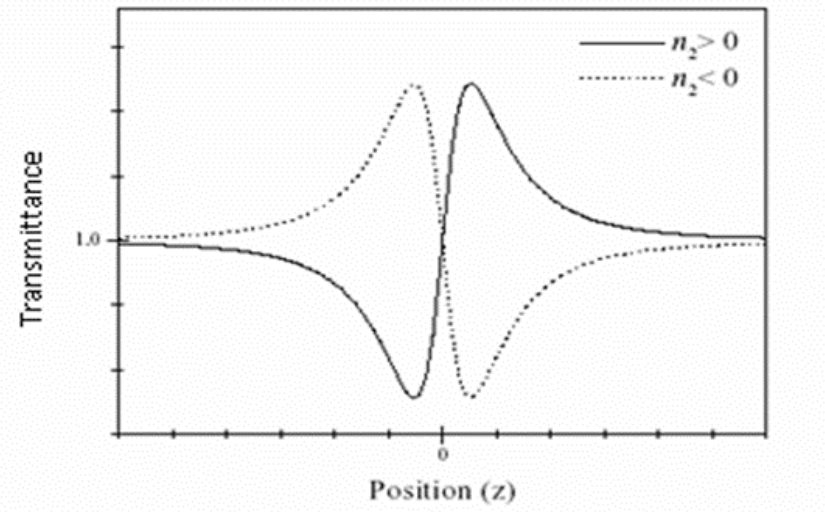

Fig.2.4: Calculated Z-scan transmittance curves for positive and negative nonlinear refractive index [70].

The nonlinear refractive index can be determined from the equation below[71]:

$$n_2 = \Delta\Phi_o / I_o L_{eff}\, k \quad (cm^2/W) \qquad (2.3)$$

Where: k is the angular wave number, equal to (2π / λ), λ is the beam wavelength, $\Delta\Phi_o$ is the nonlinear phase shift, which is calculated by the equation below[72]:

$$\Phi_o = \Delta T_{P-V} / 0.406\,(1-S)^{0.25} \qquad (2.4)$$

$$\Delta T_{P-V} = T_{max} - T_{min}$$

where $S=1-\exp(-2r_a^2/w_a^2)$ is defined as the aperture transmittance with a r_a the aperture radius and w_a the beam radius on the aperture plane[42].

L_{eff}: is the sample's effective length, which may be determined using the formula below:

$$L_{eff} = (1 - e^{-\alpha_o L}) / \alpha_0 \quad (cm) \qquad (2.5)$$

α_0 is the linear absorption coefficient, I_o is the laser beam intensity at focus, and L is the sample length, as determined by :

$$I_o = 2P_{peak} / \pi\omega_0 \qquad (2.6)$$

ω_0 is the Radius of the beam at the focal point, P_{peak} is the Laser beam power (W), which can be calculated from the equation below:

2.5.2 Open aperture Z-scan

The open aperture Z-scan technique is used to determine absorption nonlinearity. The aperture is removed from the experimental setup, and thus the entire light is collected, and the transmitted beam will touch the detector without any restriction, as shown in **Fig.2.5**.

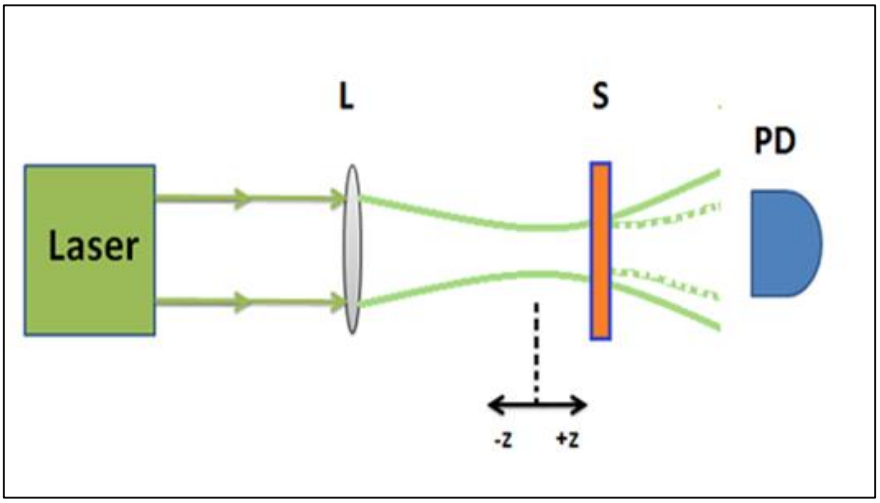

Fig2.5: Open aperture Z-scan[69].

To determine the nonlinear absorption coefficient, we assume that the total absorption follows the equation :

$$\alpha=\alpha_o+\beta I \qquad (2.7)$$

This method may be comprehended by considering a material with a thickness smaller than the diffraction length of the focused beam ($t << Zo$) and a positive absorption coefficient ($\beta > 0$). Low beam irradiance is produced by the transmitted light at the vast pre-focus area, and a relatively linear transmittance is the result of very little nonlinear absorption. A significant nonlinear absorption caused by a rise in beam irradiance causes the transmittance to decrease as the sample is pushed closer to the focus. Moving the sample causes the absorption to peak at the focus ($z=0$), where the transmittance shows a minimum and the beam irradiance is at its highest. The beam irradiance drops, and the transmittance gradually returns to its initial linear value when

the sample is pushed into the post-focus zone. The media's transmittance in the open aperture scheme is displayed in **Fig.2.6** [69].

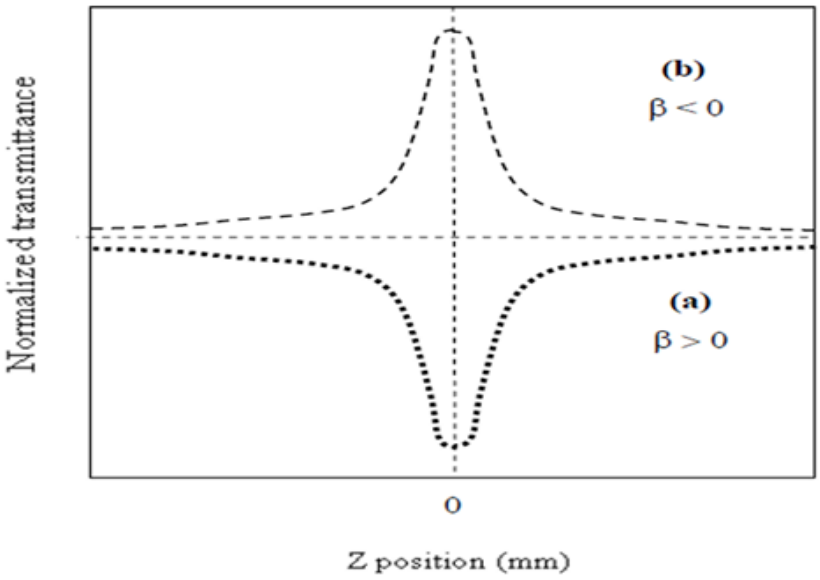

Fig.2.6: Normalized transmittance for media with (a) β > 0 and (b) β < 0 in the open aperture scheme.

The nonlinear absorption coefficient (β) can be found using the open-aperture Z-scan method from [71]:

$$T(z) = \sum_{m=1}^{\infty} \left(\frac{\left(\frac{\beta I \, Leff}{1+\left(\frac{Z}{Z0}\right)^2} \right)^m}{(m+1)^3/2} \right) \qquad \textbf{(2.8)}$$

Where: Zo is the length of diffraction, m is a number integer, Z is the position of the sample with minimal transmittance, and T(z) is the minimal transmittance.

2.6 Nonlinear Optical Techniques and Applications

2.6.1 Laser Technology

1) Nonlinear Optical Materials and Devices
2) Applications in Laser Technology

2.6.2 Telecommunications

1) Nonlinear Optical Processes
2) Material Innovations
3) Applications in Telecommunications

2.6.3 Spectroscopy & Imaging

1) Nonlinear Optical Techniques
2) Applications in Spectroscopy and Imaging

2.6.4 Medicine

1) Nonlinear Optical Techniques in Bio-Imaging
2) Applications in Disease Detection and Analysis
3) Multimodal Nonlinear Optical Microscopy

2.6.5 Sensing and Metrology

1) Nonlinear Optical Techniques in Sensing
- Enhanced Sensitivity
- Quantum Sensing.

2) Applications in Metrology
- Optical Frequency Combs
- Supercontinuum Generation

3) Integration and Future Directions
- Photonic Integration
- Optical Performance Monitoring

2.7 Zinc Oxide Nanoparticles (ZnO NPs)

Zinc oxide is one of the important metal oxides that is widely used in the industrial field, such as concrete construction, electrical and electronic devices. Interest in it has increased recently due to its important properties in exceptional

sensors, such as the change in conductivity or resistance in the presence of gas molecules, in addition to the response and recovery time[23].

The unique properties of zinc oxide, such as its ability to absorb strong ultraviolet rays, have made it an essential and effective ingredient in skin care products such as sunscreens and cosmetics. It is characterized by its anti-UV, anti-bacterial, and anti-microbial properties. Compared to other metal oxide nanoparticles, it is inexpensive and less toxic. It is effectively used in biomedical applications, such as drug delivery, antibacterial therapy, cancer control, diabetes treatment, anti-inflammatory drugs, wound healing, and bioimaging[73].

ZnO exists in multidimensional structures, including: First, one-dimensional structures such as nanorods, tubes, wires, ribbons, spirals, and nails; second, two-dimensional structures such as nanospheres or nanosheets; and third, three-dimensional structures such as nanoflowers[24].

ZnO is considered a material with excellent optoelectronic, photochemical, and piezoelectric properties. The properties of zinc oxide can be altered or enhanced by doping, surface decoration, or the formation of heterostructures for use in various other fields, such as photocatalysis. Modified particles are also used in sensing applications[74].

Zinc oxide crystallizes in two main forms: hexagonal wurtzite and cubic ZnO, as shown in **Fig.2.7(a)** and **(b)**, respectively. The wurtzite structure is more prevalent because it is more stable in environmental conditions. Zinc oxide (ZnO) can be grown on substrates with a cubic lattice structure to stabilize the ZnO structure. Tetrahedral zinc and oxide centers, which are the most distinctive structural geometry of zinc (Zn), are present in both configurations. It is under extremely high pressures that ZnO turns into rock salt. There is no inversion symmetry in hexagonal and cubic ZnO, which means that the crystals cannot be returned to their initial condition by reflection with respect to any point[75].

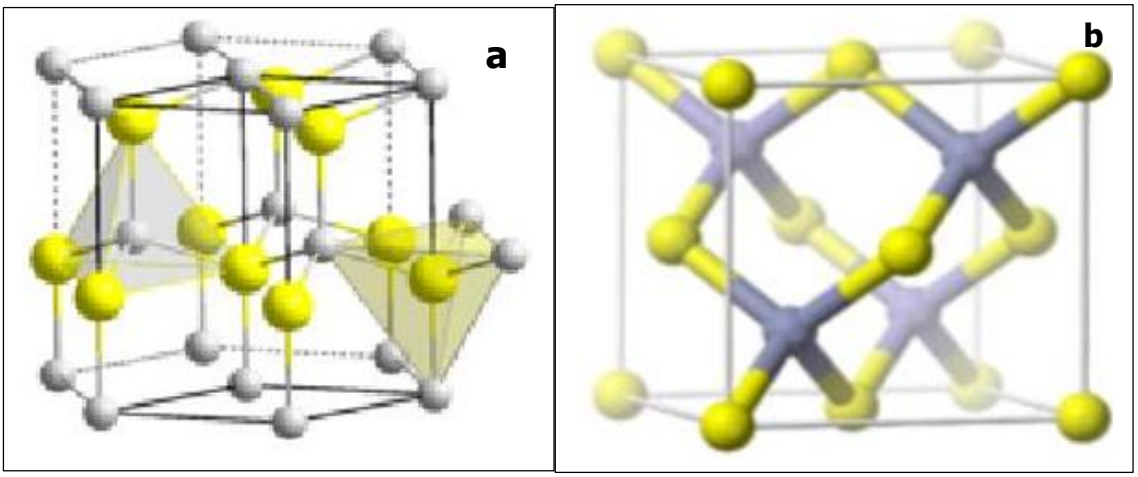

Fig.2.7: Zinc Oxide nanostructure, a) Wurtzite Structure, b) blende Unit Cell[111].

It is an n-type semiconductor with good chemical stability, characterized by a hexagonal structure with lattice parameters a = b = 3.250 Å and c = 5.206 Å [76]. It is transparent in the visible spectrum [77] and possesses a high exciton binding energy of 60 meV, allowing efficient exciton emission even at room temperature. It also has a wide direct bandgap of approximately 3.37 eV, making it suitable for optoelectronic applications in the ultraviolet and blue range. Furthermore, its low refractive index (2.05) contributes to improved light extraction efficiency, making it suitable for applications such as light-emitting diodes (LEDs) and other photovoltaic devices[78]. Furthermore, its unique optical properties allow it to emit light in the entire visible region (from violet to red)[79]. It also has two photoluminescence emissions: near-band-edge UV emission and deep-level emission associated with structural defects and impurities. It is used in advanced optoelectronic applications such as photodetectors, UV laser diodes, visible light-emitting diodes (VLEDs), and transparent thin-film transistors (TTFTs)[80].

2.8 Gold Nanoparticles (Au NPs)

Gold nanoparticles (AuNPs) are an advanced technology that has gained widespread attention in the biomedical field due to their large surface area and diverse properties compared to conventional gold. These particles have tremendous potential in medical diagnostics, drug delivery, photothermal and radiotherapy, gene therapy, and biosensing, in addition to their role in cancer control, enzyme immobilization, and cell imaging. Their applications have also expanded to include the food and beverage industries, solar cell enhancement, flash memory devices, pollution control, water and hydrogen purification, and their use as catalysts in carbon monoxide oxidation.

Although the U.S. Food and Drug Administration (FDA) has approved this technology for various medical applications, leading to its expanded use, its increasing use raises concerns about the potential for human exposure to these particles. Multiple studies from academic and commercial sources have revealed potential toxic effects that warrant further research and evaluation[81].

Gold nanoparticles (Au NPs) exhibit the ability to interact with light through the localized surface plasmon resonance (LSPR) phenomenon, as shown in **Fig.2.8(b)**, giving them unconventional optical properties and potentially being used as active components in future optical and plasmonic devices [82].

In the nanoscale, the surface-to-volume ratio increases significantly, and thus the physical and chemical properties of materials change, differing markedly from those of their normal-sized counterparts. For example, gold nanoparticles with a diameter of less than 100 nm suspended in water have a ruby red color instead of gold. This is due to the surface plasmon resonance (SPR) phenomenon, which refers to the oscillation of the free electrons of the nanoparticles when excited by incident light[83].

These unconventional optical properties are due to the localized surface plasmon resonance (LSPR) phenomenon, which arises as a result of the oscillation of free electrons in metallic nanoparticles when exposed to

electromagnetic waves (EMWs). This interaction creates a charge distribution at the interface between the nanoparticle and the surrounding dielectric medium, due to the dielectric confinement effect. These conditions induce localized electrical and magnetic oscillations. When the frequency of the incident wave matches the frequency of these oscillations, resonant absorption occurs at a specific wavelength known as the LSPR wavelength, which is highly sensitive to the particle's size, shape, and composition, as well as the surrounding medium[84].

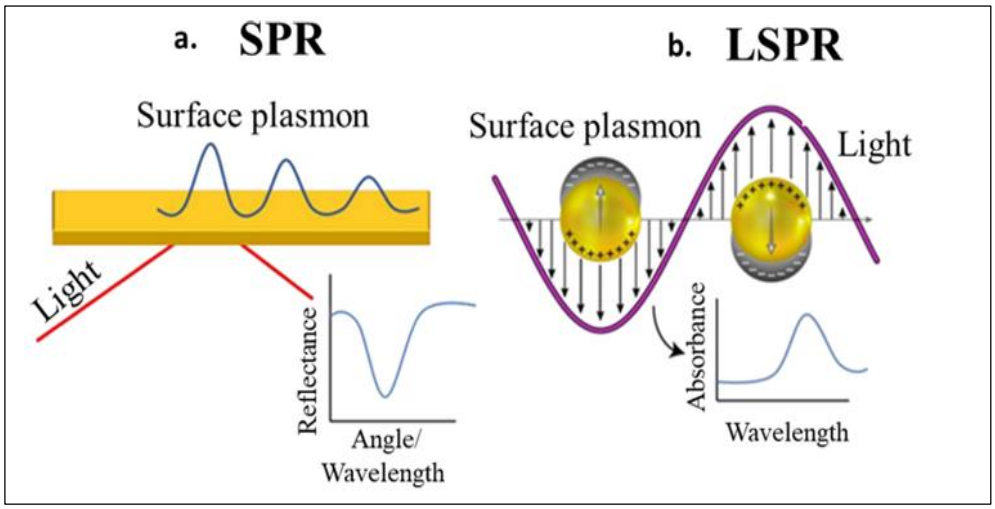

Fig.2.8: (a) surface plasmon resonance (b) Localized surface plasmon resonance[85].

2.9 Preparation of Nanoparticles:

Nanoparticle synthesis techniques can be divided into two categories: top-down and bottom-up strategies. Top-down methods rely on the fragmentation of bulk material to produce nanoparticles and include methods such as ball milling, sputtering, and thermal evaporation. In contrast, bottom-up methods involve constructing nanoparticles by combining their atomic elements, often performed using chemical synthesis techniques such as co-precipitation, sol-gel, hydrothermal deposition, and chemical vapor deposition. Laser ablation, which will be explained later, is generally considered a top-down technique for

nanoparticle synthesis, as it uses laser energy to ablate bulk material and produce nanoparticles. However, this technique can also be considered a bottom-up approach because nanoparticles are subsequently formed via nucleation and growth of material elements resulting from intense pulsed laser interaction[86].

2.9.1 Preparation of nanoparticles by laser ablation

Pulse laser ablation in liquid (PLAL) is used to prepare nanostructures by removing material from a solid target in a liquid during laser-matter interaction. The final shape and properties of the nanomaterial depend on the laser's interaction with the material and other parameters such as the nature of the solvent, the solid target background, the laser pulse width and duration, and the laser beam optics[87].

When a high-energy laser beam is focused onto a solid material or target fully immersed in a liquid, the temperature and pressure on the target surface rise suddenly and rapidly over a very short period of time. As a result, a portion of the metal surface evaporates, forming what is known as a plume. Atoms, ions, and clusters of particles then travel rapidly toward the liquid and interact with its molecules, resulting in the formation of new nanoparticles[21].

The scientific community is still engaged in a vigorous debate regarding the fundamental aspects of nanoparticle synthesis, as the physicochemical processes involved in PLAL are not completely comprehended or understood.

The laser's interaction with matter generates a high-temperature plasma with a substantial density of species (atoms, ions, and electrons) that serves as the solid's source; this plasma energy subsequently transfers to the surrounding liquid, creating a cavitation bubble marked by expansion and collapse dynamics; ultimately, nanoparticles are released into the liquid[88].

This new method has gained significant attention due to its significant advantages, such as its environmental sustainability, the simplicity of its

experimental setup, which does not require harsh preparation conditions, and its ability to produce stable nanoparticles that are completely free of pollutants or hazardous chemicals [89]. This method is called "green synthesis" because it requires no chemicals, making it a clean and byproduct-free technique. Not only the metallic materials are used in the preparation of colloidal nanoparticles, but a variety of materials can be used, such as ceramics, magnetic materials, semiconductors, insulators, conductors, composites, organic materials, and hybrid materials[90]. The liquid medium in this technology offers several advantages by controlling the dynamic process of plasma-free motion. First, the liquid restricts plasma expansion, concentrating energy and generating extreme conditions characterized by elevated temperatures and pressures. Second, the plasma quenching duration in a liquid medium is reduced, resulting in a constrained timeframe for nanoparticle (NP) material to develop into bubbles, hence ensuring uniform product size. Finally, nanoparticles are more readily collected in liquid settings[91].

Shock waves, cavitation bubbles, and visible plasma emission are the hallmarks of laser-induced breakdown of submerged objects. The following is an explanation of the fundamental procedures that take place during the PLAL method to create nanoparticles:

1- Laser–matter interaction

Upon the instance a concentrated, pulsed laser beam impacts the surface of a solid target, it transmits a remarkably high power density, usually surpassing 10^6 W/cm². The substance absorbs this energy, stimulating electrons or electron–hole pairs contingent on its composition, either metallic or semiconducting. On ultrafast timeframes, the excited electrons relinquish their energy to the lattice, leading to swift heating of the surface layer. Dependent on the laser pulse duration, fluence, and the material's thermal and optical characteristics, the ablation might proceed through thermal mechanisms such as vaporization or boiling, or through non-thermal pathways involving direct

structural alterations. This initial interaction phase dictates the conditions wherein plasma will form, signaling the shift from solid to a dense, hot plasma condition[92]. **Fig.2.9** shows the experimental configuration of PLAL.

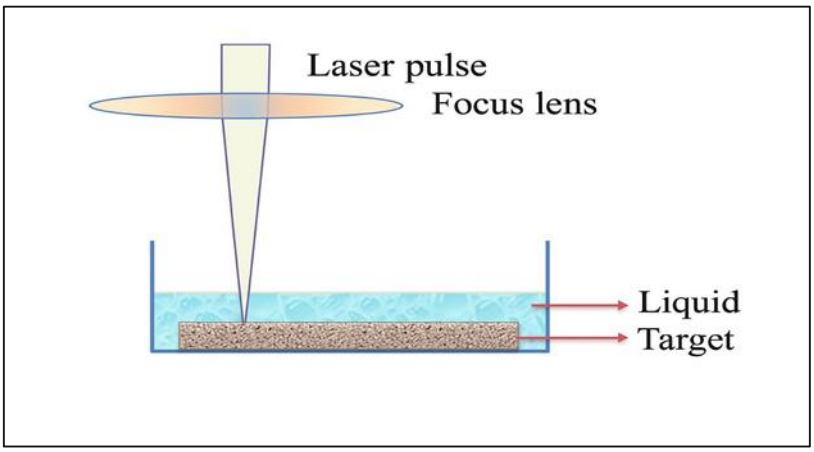

Fig.2.9: A diagram illustrating the experimental configuration of PLAL[92].

2- Plasma formation

Upon interaction of laser pulses at an irradiance of (0.1–1 GW/cm^2) with a solid target, multiphoton ionization releases seed electrons, and absorption of photons by inverse bremsstrahlung generates a heated atomic plasma. In ablation, the material density alters constantly across the solid–gas phase transition, at first, forming an exceedingly dense, hot plasma[89].

3- Shock wave generation

As demonstrated, the plasma expands supersonically, producing a shock wave before slowing down beneath the surrounding liquid pressure until extinction, as shown in **Fig.2.10**. Within liquids, the main functions maintaining plasma are akin to those in air, yet they vary in the equilibrium of procedures and energy transfer with the medium. Because of the fluid's minimal compressibility, the plasma is contained, preserving a density of approximately 10 and ionization close to one. The Debye–Hückel influence constrains excited states, rendering radiative recombination predominant and resulting in continuous emission spectra akin to a Planck distribution, which allows for plasma temperature

determination. Observed laser-created plasma temperatures in water vary between 4000 and 6000 K[89].

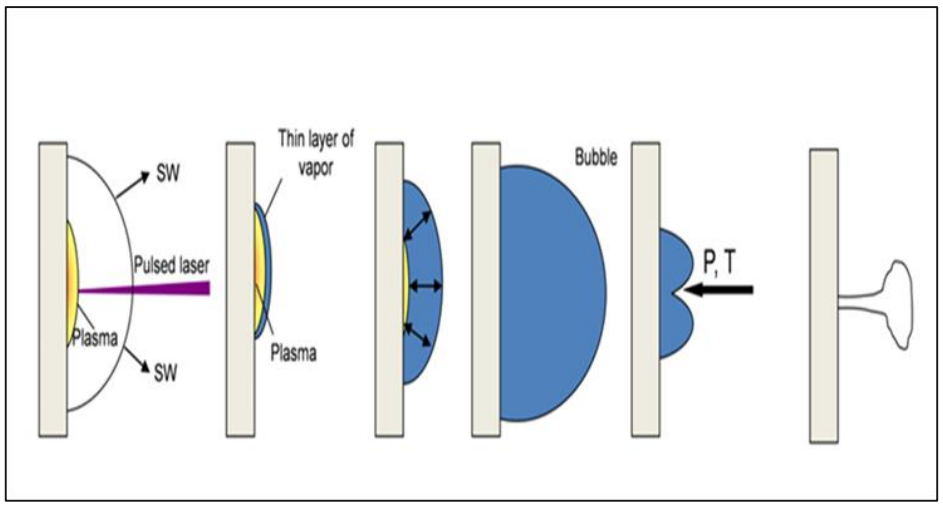

Fig.2.10: The basic processes that occur during the PLAL[89].

4- Cavitation bubble formation

Heat is rapidly transferred into the surrounding liquid, resulting in a phase change of the liquid that touches the plasma front. This forms the first bubble, which is a thin film of vapor surrounding the plasma region. This layer forms at high temperature and pressure and spreads out in every direction, forming a cavitation bubble, and the plasma is also contained in this layer. The bubble lifespan is also numerically dependent on the laser pulse properties; they are the wavelength, the output energy, and the focusing settings, the pulse duration, and the outside pressure; the bubble lifespan is normally in the hundreds of microseconds, twice the plasma duration itself. Bubble dynamics consist of a phase of growth and of decay, and can recur, like a damped oscillator. When the fluid pressure in the bubble reaches the saturation point temperature, the bubble has the maximum radius and can withstand longer than in the contraction and collapse periods in a quasi-equilibrium state. This provides the engineered nanoparticles with more time and space to proliferate, hence lowering their local concentration [89].

5-Nanoparticle nucleation and growth

The generated material is drawn into the bubble volume during the expansion stage as a bubble forms at the plasma contact. The nanoparticle is enclosed inside the bubble because the expansion rate is greater than the diffusion rate. The bubble has the lowest concentration of nanoparticles throughout its whole growth when it reaches its greatest size, when its volume might be up to two orders of magnitude higher than its original size. The bubble begins to gradually contract after the stage of maximum growth, and the radius changes at the same rate as during the expansion but in the opposite direction (decreasing rather than expanding), as seen in **Fig.2.11**.

Throughout the implosion stage, the particles are impelled toward the target and gather at the bubble's edge. They are subsequently released into the fluid upon implosion completion. The spread of these particles inside the bubble can be monitored with a second laser burst to produce a subsequent plasma of the ejected material. The energy of the second pulse hitting the target depends on the particle density within the focal region. During the expansion stage, much of the energy is consumed in nanoparticle breakdown inside the bubble. At equilibrium, a significant amount of the particles diffuse, and their density decreases, allowing most of the energy to be delivered onto the target, prompting additional ablation. During the implosion phase, the particles concentrate in front of the target, hindering the second pulse and causing their breakdown at the point of accumulation[89].

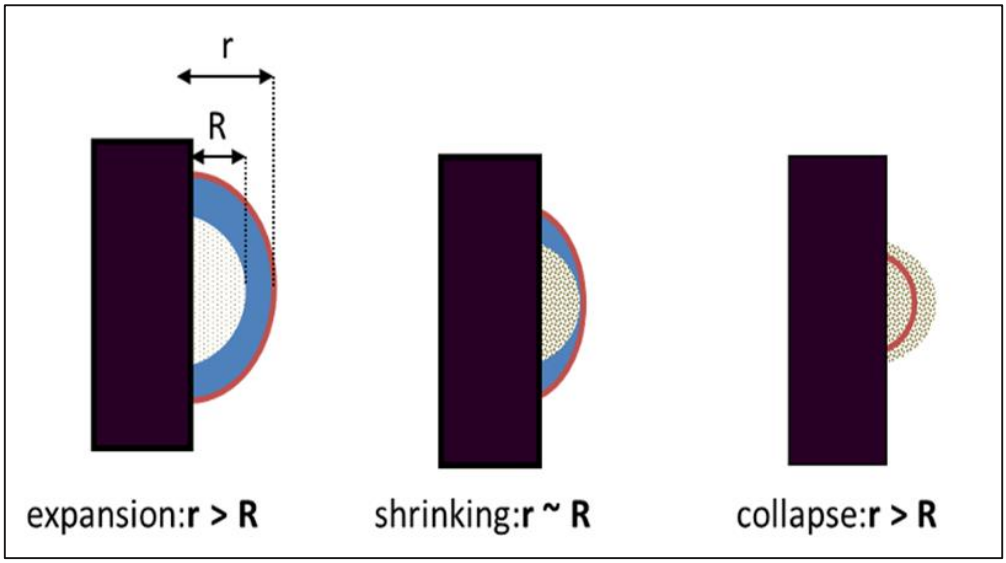

Fig.2.11: The NPs cloud and bubble size during different phases of the bubble lifetime: The bubble and NPs cloud radii are denoted by r and R, respectively[89].

2.10 Photocatalysis Activity

Photocatalysis utilizes photon energy to promote reactions through mechanisms distinct from thermal or electrocatalytic processes. When designed correctly, it can catalyze energetically unfavorable reactions under mild conditions. It is advantageous as it can function as a really passive process with minimal chemical input. The process of photocatalysis in semiconductor materials commences with the absorption of a photon with an energy that exceeds the optical bandgap. The energy of the photon is absorbed, which facilitates the transfer of an electron from the valence band (VB) to the conduction band (CB). This process leaves a cavity in the VB and places an electron in the conduction band. The electrons and holes that are produced by the photon can be utilized in oxidation and reduction reactions, respectively. The efficiency of photocatalysis is, however, intrinsically constrained by the rapid recombination of charge carriers and the low absorption of the solar spectrum[93].

Throughout the past few decades, multi-component photocatalytic methods for dealing with organic contaminants utilizing semiconductor nanoparticles have garnered growing interest as it represents an economical, eco-friendly, and simple approach for remediating wastewater holding dangerous pollutants. The inexpensive nature of catalysts and the employment of sustainable power in this method are considerably more appealing than alternative techniques. Photolysis is an oxidation procedure where the chemical breakdown of intricate compounds converts into basic, innocuous, low-mass pieces via exposure to light. This is an evolving and promising procedure for wastewater cleanup, able to remove color and break down dye molecules into simple, safe inorganic substances like carbon dioxide and water. The reaction occurs alongside a photocatalyst, a semiconductor substance activated by absorbing light quanta, which can speed up the process without depletion. MB is a firm powder, scentless, dark green at ambient temperature, and produces a blue liquid when mixed in water. It is a typical organic colorant and stable under visible light irradiation. Due to its stability, it cannot be effectively broken down by photolysis or catalysis in isolation.

Photodegradationof MB is an effective approach because it can alsoserveas a photocatalyst. Theslight/partialbreakdownseenin MB without catalysts can becreditedto thelight-sensitivenature of MB molecules, which isapparentafterexposuretovarious light sources. MB cantakeinlight in the 500–700 nm range,createsingle and triple species via electron transfer and intersystem transition, andexperiencesomeextentofself-cleavage[94].

The increasing level of pollution in industrial wastewater, especially organic dyes, requires the use of advanced materials capable of harnessing solar energy to efficiently decompose pollutants. Among these materials are zinc oxide (ZnO) nanoparticles, which are promising semiconductors due to their wide band gap, large exciton binding energy, good chemical stability, and non-toxicity. These advantages make ZnO nanoparticles an ideal choice for

photocatalysis and the removal of various organic pollutants, including hazardous dyes such as methylene blue (MB) and rhodamine B (RB). Despite its great potential, the photocatalytic efficiency of pure ZnO is limited by two main factors: its poor light absorption in the visible range and the rapid recombination of photogenerated electron-hole pairs, which reduces its effectiveness in solar radiation[95].

To reorganize the above issues in photocatalytic applications, some researchers have modified the surface of nanostructured ZnO with semiconductor coverings or metal nanoparticles to eliminate the recombination of charge carriers produced by optical excitation and to extend the photo-response range to the visible light range. In the preparation of ZnO-metall nanocomposites that have high photocatalytic properties, gold is a popular metal used in tuning the surface of nanostructured ZnO. The local surface plasmon resonance (LSPR) effect causes the electrons on the Fermi levels of Au and lower to be resonantly stimulated to higher levels. However, the reported photocatalytic activity of the Au nanoparticle modified ZnO (ZnO-Au) nanocomposites is diverse and may vary within a wide range depending on the size and shape of Au nanoparticles, as well as the methods used to prepare ZnO-Au nanocomposites[96].

2.11 Characterization of Examination Sample

2.11.1 X-ray Diffraction Technique

X-ray diffraction (XRD) is an important and popular technique used to characterize materials. XRD patterns are utilized in investigating, exhaustively, any issues relating to crystal structure, grain size, orientation, dislocation density, phase identification, quantification, and transformation, including peculiarities of lattice parameters, residual stress and strain, as well as the coefficient of thermal expansion of materials [97]. It is a nondestructive and highly useful laboratory procedure used to perform the investigation of most types of materials: fluids, metals, minerals, polymers, catalysts, plastics,

pharmaceutical drugs, thin-film coating, ceramics, solar cells, and semiconductors. The methods of this technique are widely used in many industries: microelectronics, power generation, aerospace, and so on. X-ray diffraction analysis can give a crystal's constitution, whether it be the presence of defects, stress level, texture, size, degree of crystallinity, or practically any other variable in the basic structure of the given sample [98], as present in **Fig2.12.**

The distance between atomic planes in a lattice can be measured using Bragg's law and using equation (2.10)

$$n\lambda=2d \sin \theta \qquad (2.9)$$

Where: λ is X-ray wavelength, θ is diffraction beam angle, n is the order of reflection (diffraction), and d is the spacing between atomic planes. The crystallite size can be calculated using the Scherrer equation.

$$D=K \lambda/B \cos \theta \qquad (2.10)$$

Where: K is the Scherrer constant = 0.9, λ is the XRD wavelength, and D is the crystallite size, B is the full width at half maximum (FWHM) measured in radians, θ is the diffraction angle[97].

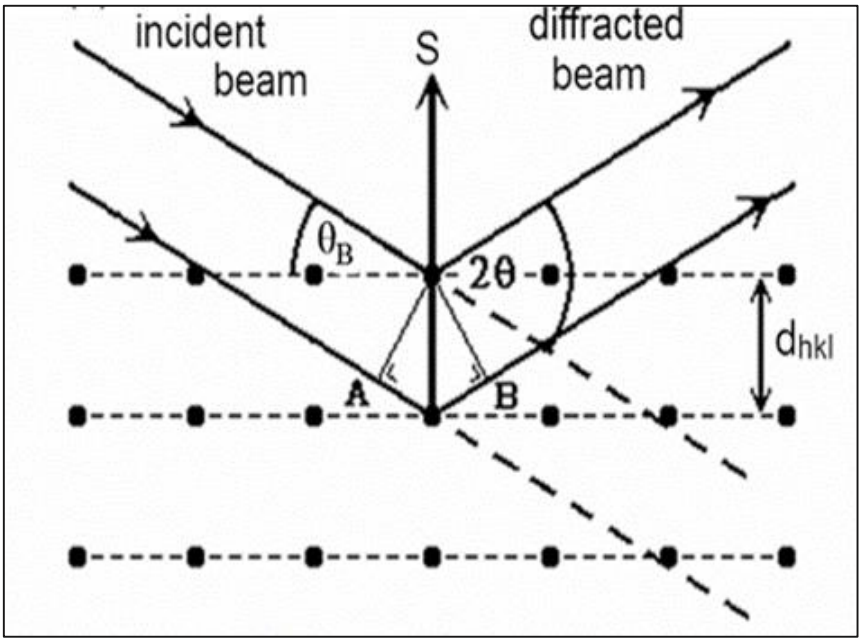

Fig.2.12:Bragg's law[99].

2.11.2 Energy Dispersive X-Ray Analysis (EDX)

It is used to measure the elemental composition of nanoparticles using a scanning electron microscope. In a standard scanning electron microscope, materials interact with the electron beam when it strikes them, producing distinctive X-rays. Because each element in a sample has its own unique X-ray emission spectrum, its concentration can be measured and characterized. X-rays are produced when an electron beam interacts with a sample. This excites and dislodges one of the inner electrons, creating an electron hole that is filled by an electron from a higher energy level within the atom. This transition results in the emission of a photon in the form of an X-ray. The resulting X-rays are divided into two types: characteristic X-ray (generated as a result of higher shell electron filling the electron hole in the nucleus shell) and X-ray, which consists of X-ray continuum (generated by the deceleration of electron)[100].

2.11.3 Field Emission Scanning Electron Microscopy (FESEM)

FE-SEM is a powerful and widely used technique for studying the microstructure of cells and tissues[101].

The microscope's working principle is to fire electrons from an electron ball, which is considered an electron source (called an electron gun), in the form of a stream of electrons. These are directed at the specimen to be examined by a magnetic lens, and the surface is examined in three dimensions to produce a three-dimensional image that includes all the details of cracks, scratches, and gaps. When the electron beam is examined (a magnetic field with a variable potential difference is used to control the movement of the electron beam over the specimen), it interacts with the specimen surface and ejects electrons. These are finally detected by the detector (FE-SEM detector), which images the scattered electrons [102]. **Fig.2.13** shows the parts of (FE-SEM).

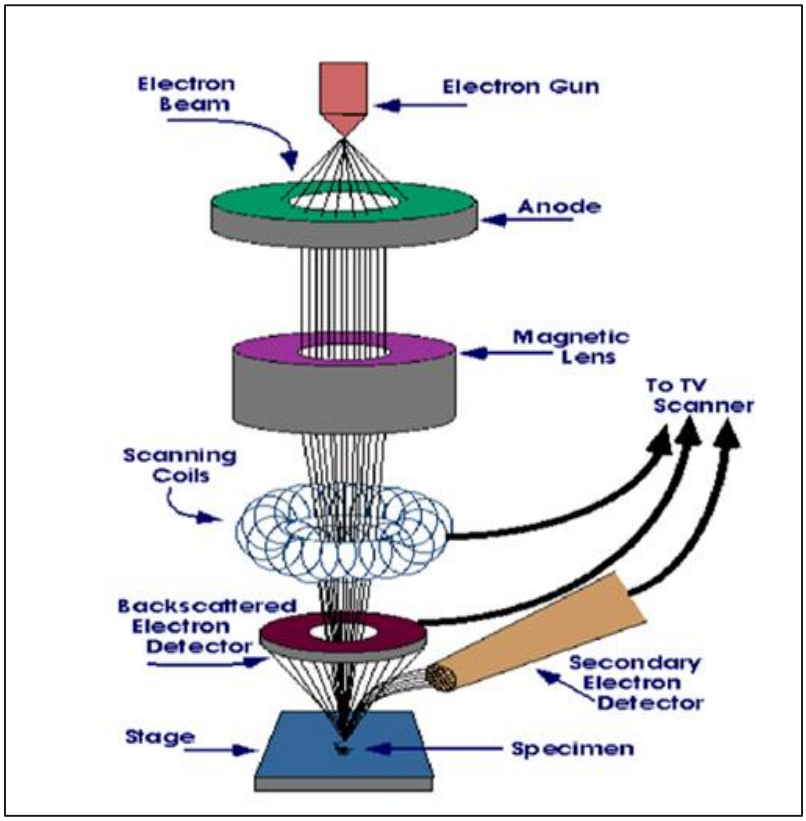

Fig.2.13: Schematic diagram of Field Emission Scanning Electron Microscopy[102].

It provides ultra-high-resolution images with low accelerating voltage, short working distance, and image resolution as low as (0.6 nm) at 15 kV and (1.2 nm) at 1 kV, enabling us to examine the top surface of nanopowders, nanofilms, and nanofibers used in various applications, such as chemistry, physics, life sciences, ceramics, polymers, metallurgy, and electronic devices [103].

2.11.4 UV-visible Absorption Spectroscopy

UV-Vis spectroscopy is a rapid analytical method used to determine the transmittance or absorption of light. Most spectrophotometers operate in the wavelength range of 200-1100 nm, although the wavelengths of UV and visible light are 100–380 nm and 800 nm, respectively. The practical UV-Vis range is approximately 200-800 nm; the infrared range is 800 nm and above, while the vacuum UV range is 200 nm and below. The color of a material is determined

by its ability to absorb and emit light, and the human eye can distinguish up to 10 million different colors. Light passes through (transmissive) media, is reflected by opaque and transparent surfaces, and is refracted by crystals [104].

UV-Vis spectroscopy is based on the Beer-Lambert law, which states that the absorbance is exactly proportional to both its route length and the concentration in the solution. As a result, it can be utilized to ascertain the adsorbent concentration in a solution at a constant route length. When radiation induces an electronic transition in a molecule's or ion's structure, the molecule or ion shows absorption in the visible or ultraviolet spectrum. As a result, when a sample absorbs light in the visible or ultraviolet spectrum, the electronic state of the molecules within the sample changes. Electrons are propelled from their ground orbitals to higher-energy orbitals, also known as excited orbitals or antibonding orbitals, by the energy that the light provides [105], as present in **Fig.2.14**.

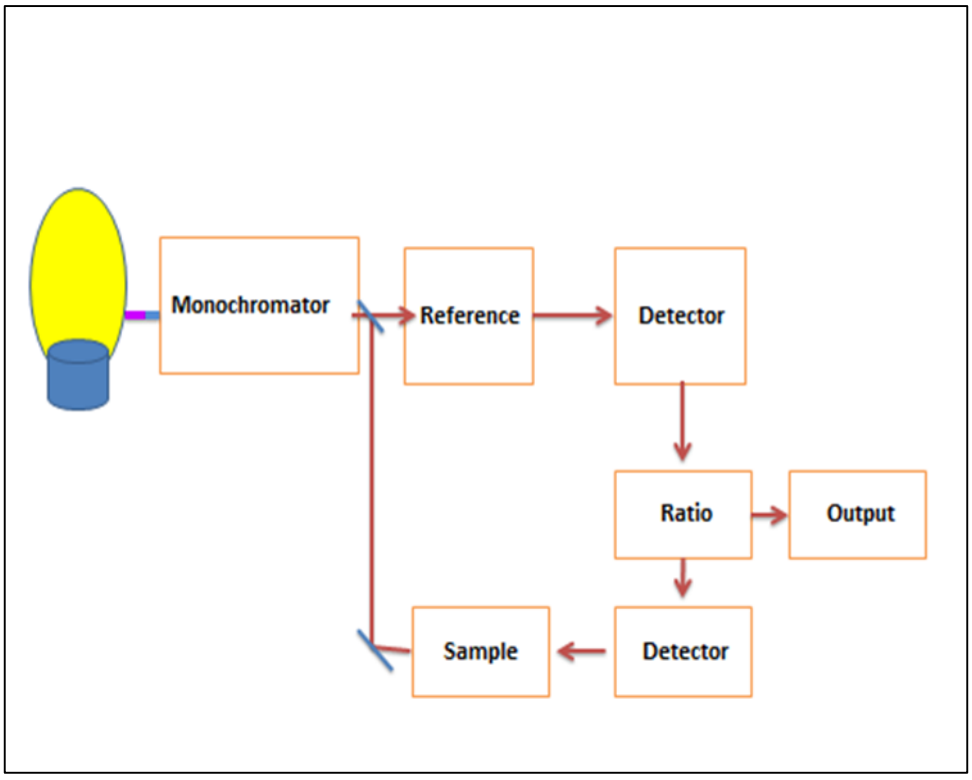

Fig.2.14: Instrumentation of UV-Spectroscopy.

2.11.5 Transmission Electron Microscopy (TEM)

A transmission electron microscope (TEM) is a microscopic instrument that produces an image by passing beams of electrons through a specimen. To use this device, the specimen must be prepared on a transmission electron microscope grid and placed in the center of the microscope chamber. The microscope produces the image using fluorescent screens. This microscope is intended to examine the internal and external structure of the specimen[106].

The electron beam interacts with the sample as it passes through it, and an image is formed by the transmitted electrons. This image can be magnified and focused using an objective lens. Diffraction rather than absorption occurs when the electron beam interacts with the sample; this is the difference between a transmission electron microscope image and an optical microscope image. Changing the orientation of the plane relative to the electron beam will change the diffraction intensity. At some angles, the electron beam deviates sharply from the axis, while at other angles it will shift. To obtain a specific diffraction condition, specimen holders are mounted so that they can be tilted to suit the desired condition. Positioning the aperture to block scattered electrons and allow the passage of unscattered electrons, using these electrons to produce a contrasting image, is known as a (light field). Scattered electrons can be used to produce an image known as a dark field image. **Fig.2.15** shows the components of a transmission electron microscope [107].

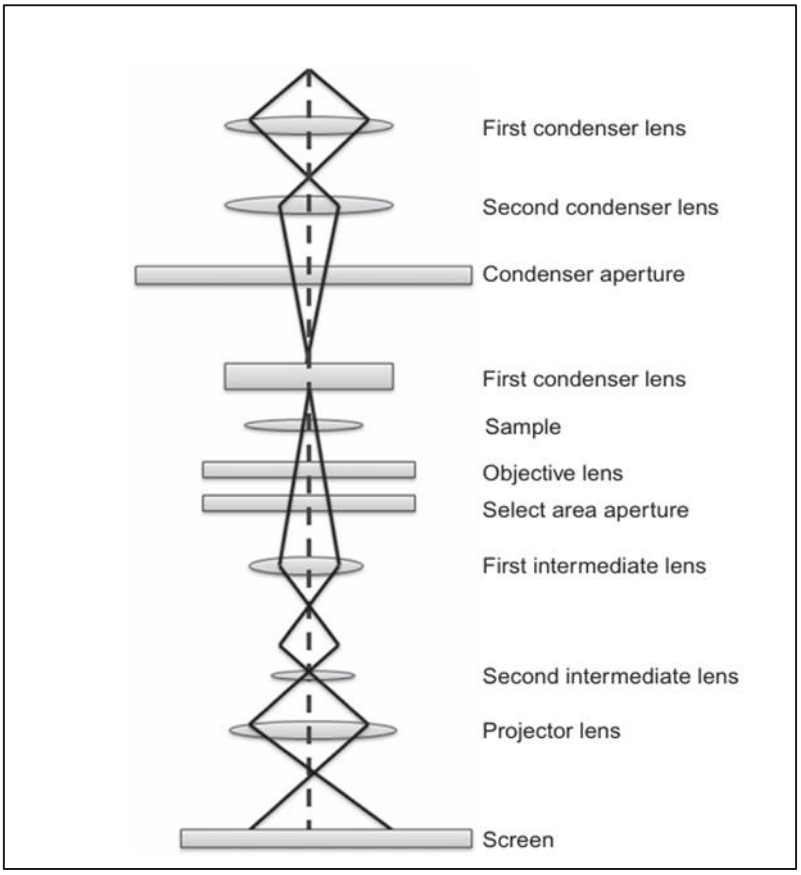

Fig.2.15:Basic components of Transmission Electron Microscopy (TEM)[107].

2.11.6 Fourier Transform Infrared Spectroscopy (FTIR)

A spectrophotometer is a tool used to measure a compound's absorption spectrum. A Fourier transform spectrophotometer (FTS) provides infrared spectra far more quickly than a traditional spectrophotometer. A brilliant blackbody source inside the gadget emits an infrared radiation beam. After that, an interferometer is used to encode the beam's spectrum. When beams of varying path lengths recombine in the interferometer, constructive and destructive interference result, creating an interference pattern. The beam then enters the sample chamber, and the sample will absorb specific energy frequencies and appear in the interferogram. The detector then detects the particular interferogram signal in terms of energy against time for all frequencies concurrently. In the meantime, a beam is added to provide the

gadget a reference, or backdrop, on which to function. The required spectrum is acquired when the interferometer uses a Fourier transform computer software to automatically remove the background spectrum from the sample spectrum. The fundamental parts of a basic Fourier transform spectrophotometer are shown in Fig.**2.16** [108].

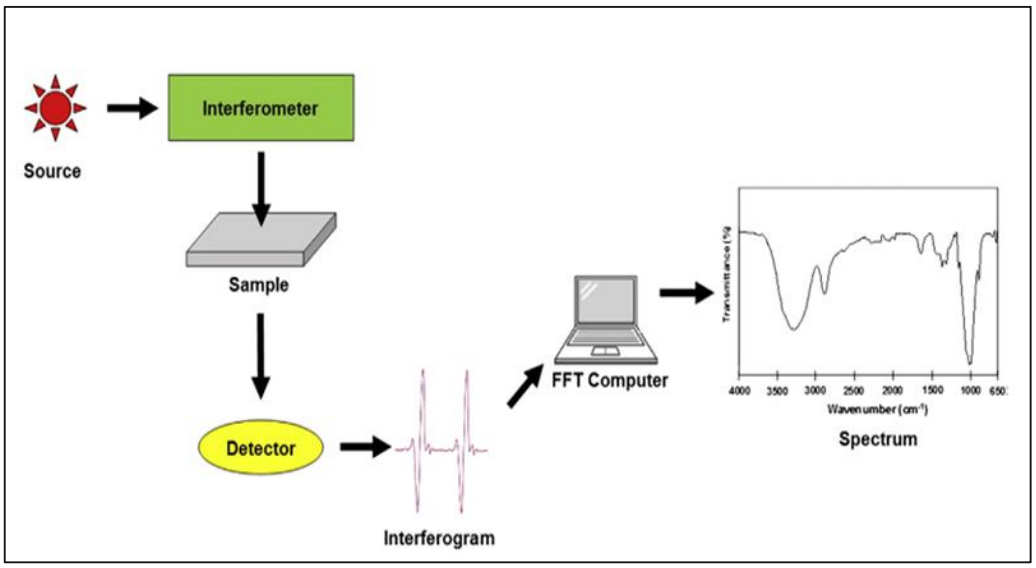

Fig.2.16:Basic component in Fourier transform infrared spectrometer(FTIR)[108].

الخلاصة:

في هذا العمل، تم تصنيع جسيمات نانوية من أوكسيد الزنك (ZnO) والذهب (Au) إضافة إلى الجسيمات النانوية المركبةZnO–Au باستخدام تقنية الاستئصال بالليزر النبضي في السوائل (PLAL) باستعمال ليزر Nd:YAG بطول موجي 1064 نانومتر. تمتاز هذه الطريقة ببساطتها وسرعة الحصول على الجسيمات النانوية خلال فترة زمنية قصيرة وبتكلفة منخفضة، فضلاً عن ضمان نقاء عالٍ وظروف صديقة للبيئة أثناء التصنيع.

تمت دراسة الخصائص البنيوية والمورفولوجية والبصرية اللاخطية إضافة إلى الصفات التحفيزية الضوئية للجسيمات المحضّرة باستخدام طرق مختلفة. أظهرت نتائج حيود الأشعة السينية (XRD) الأطوار البلورية للمواد النانوية، مع حساب متوسط الحجم البلوري باستعمال معادلة شيرير. أما تحليل مطيافية الأشعة السينية المشتتة للطاقة (EDX) فقد أكد التركيب العنصري للعينات، موضحًا وجود العناصر المتوقعة فقط مما يثبت نقاء الجسيمات النانوية المصنعة. في حين أظهرت صور المجهر الإلكتروني الماسح الميداني (FESEM) والمجهر الإلكتروني النافذ (TEM) الأشكال المميزة لكل عينة: جسيمات ذهبية كروية، جسيمات ZnO سداسية الشكل، وهياكل نانوية ZnO–Au .

أوضحت أطياف الامتصاص في المجال فوق البنفسجي–المرئي (UV–Vis) الرنين السطحي للبلازمونات المميز للجسيمات الذهبية والحافة الامتصاصية الواضحة لأوكسيد الزنك، مع تغيرات طيفية ملحوظة في العينة المركبة ZnO–Au تعزى إلى اقتران البلازمون مع شبه الموصل. كما أكدت نتائج مطيافية الأشعة تحت الحمراء بتحويل فوريه (FTIR) وجود المجموعات الوظيفية والروابط المميزة ضمن الهياكل النانوية.

تمت دراسة الخصائص البصرية اللاخطية من المرتبة الثالثة باستخدام تقنية Z-scan في وضعي الفتحة المغلقة والمفتوحة عند طول موجي 532 نانومتر. وأظهرت النتائج أن الجسيمات النانوية–ZnO Auتمتلك قابلية بصرية لاخطية أعلى($\chi^{(3)}$) ، ومعامل انكسار لاخطي(n_2) ، ومعامل امتصاص لاخطي (β)مقارنة بجسيمات ZnO أو Au النقية. كما أظهرت العينات خاصية التركيز الذاتي للشعاع (n_2 موجب (والامتصاص المشبع عند شدة معينة، ويُعزى ذلك إلى تأثير رنين البلازمون السطحي الموضعي (LSPR)للذهب وتحسين انتقال الشحنة عند واجهة المعدن–شبه الموصل.

تم تقييم الكفاءة التحفيزية الضوئية عبر دراسة تفكك صبغة الميثيلين الأزرق (MB) تحت أشعة الشمس. أظهرت جسيمات ZnO–Au كفاءة تحلل أعلى مقارنة بجسيمات ZnO أو Au النقية، حيث بلغت 91%. ويعزى ذلك إلى التأثير التآزري بين زيادة الامتصاص الضوئي بفعل ظاهرة البلازمون في الذهب والنشاط التحفيزي لأوكسيد الزنك. كما ساهمت إضافة جسيمات الذهب في توسيع مدى الامتصاص الطيفي وتقليل إعادة اتحاد أزواج الإلكترون–الفجوة، مما أدى إلى تحسين ملحوظ في الأداء التحفيزي الضوئي.

بشكل عام، توضح هذه الدراسة أن الهياكل النانوية ZnO–Au المُحضَّرة بتقنية PLAL تتميز باستقرار بنيوي عالٍ، وخصائص بصرية قابلة للضبط سواء خطية أو لاخطية، وكفاءة تحفيزية ضوئية ممتازة، مما يجعلها خيارات واعدة للتطبيقات في الأجهزة الفوتونية، ومحددات القدرة الضوئية، وتنقية الملوثات البيئية. وتؤكد النتائج إمكانات تقنيات التصنيع بالليزر الصديقة للبيئة لإنتاج مواد نانوية متقدمة متعددة الوظائف.

جمهورية العراق
وزارة التعليم العالي والبحث العلمي
جامعة ديالى
كلية العلوم
قسم الفيزياء

توليف جسيمات Zno:Au النانوية المحضرة بالاستئصال بالليزر في السائل لتطبيقات التحفيز الضوئي

رسالة
مقدمة الى مجلس كلية العلوم جامعة ديالى وهي جزء من متطلبات نيل
درجة الماجستير في علوم فيزياء الليزر
تقدمت بها

حنان خالد عوده
بكلوريوس علوم الفيزياء-فيزياء الطبية
كلية العلوم /جامعة ديالى (٢٠٢٠)

بأشراف:
أ.د.نادية محمد جاسم

١٤٤٧هجري ٢٠٢٥ميلادي